Energy Management in Autonomous Microgrid using Stability-Constrained Droop Control of Inverters

E. Barklund, Nagaraju Pogaku, Milan Prodanović, *Member, IEEE*, C. Hernandez-Aramburo *Member, IEEE*, Tim C Green, *Senior Member, IEEE*

Department of Electrical and Electronic Engineering, Imperial College London, UK

Contact Address/Corresponding Author:

Dr. Nagaraju Pogaku

Dept. of EEE, Imperial College London

South Kensington, London SW7 2AZ, UK

Phone: +44 (0)20 7594 6295

Fax: +44 (0)20 7594 6282

e-mail: nagaraju.pogaku@imperial.ac.uk

Prior Presentation: IEEE International Conference on System of Systems Engineering 2007

Abstract: This paper presents an Energy Management System (EMS) for a stand-alone droop-controlled microgrid, which adjusts generators output power to minimize fuel consumption and also ensures stable operation. It has previously been shown that frequency-droop gains have a significant effect on stability in such microgrids. Relationship between these parameters and stability margins are therefore identified, using qualitative analysis and small-signal techniques. This allows them to be selected to ensure stability. Optimized generator outputs are then implemented in real-time by the EMS, through adjustments to droop characteristics within this constraint. Experimental results from a laboratory-sized microgrid confirm the EMS function.

*Index terms:*Microgrids, Energy Management System (EMS), droop control, small-signal stability.

I. Introduction

Microgrids have received increasing attention as a means of integrating distributed generation such as Combined Heat and Power (CHP) into the electricity network. Usually described as confined clusters of loads, storage devices and small generators ($<$ 500kW), these autonomous networks connect as single entities to the public distribution grid [1] [2] [3]. The low-voltage non-50/60Hz power output of many forms of small-scale distributed generation - including wind turbines, fuel cells, reciprocating gas engines and energy storage - means that power-electronic converter interfaces are required. While such low-inertia interfaces tend to make microgrids sensitive to disturbances, they enable flexible operation of the connected generators [4], [5].

Real-time optimization is therefore feasible in microgrids, through frequent adjustments of generator outputs to minimize costs or meet other targets [6]. Optimization may include power flow to the public network: energy for storage can be bought when prices are low, and then used when the grid connection is unavailable. Energy Management Systems (EMS) have been proposed to coordinate such functions [7] [8] [9] [10] [11] [12].

An important consideration when implementing optimal generator outputs is system stability. When the microgrid is operated in stand-alone mode, its dynamics are strongly dependent on the connected sources and on the power regulation control of the converter interfaces [4], [5]. This is similar to a conventional grid where the system stability is largely influenced by the synchronous generators. For droop-controlled microgrids, which offer advantages in terms of autonomous operation, analysis has shown that the parameters that determine generator power sharing have a significant effect on stability in stand-alone operation [4]. A deeper understanding of this effect is required, to allow an EMS to apply real-time optimization. This paper presents the application of small-signal stability analysis, previously developed in [4], to an EMS for a laboratory-size droop-controlled microgrid. Experimental results have been collected to validate the proposed control strategy.

II. Microgrid structure

The laboratory microgrid under study, which is fully described in [4] and [13], has three distributed generators (DG) with 10kW inverter interfaces, and two local load buses, as shown in Fig. 1 (a). Each DG is represented by a DC supply. Inverter power controllers regulate the real and reactive power outputs, by providing reference values for the output voltage magnitude and phase. These references are based on

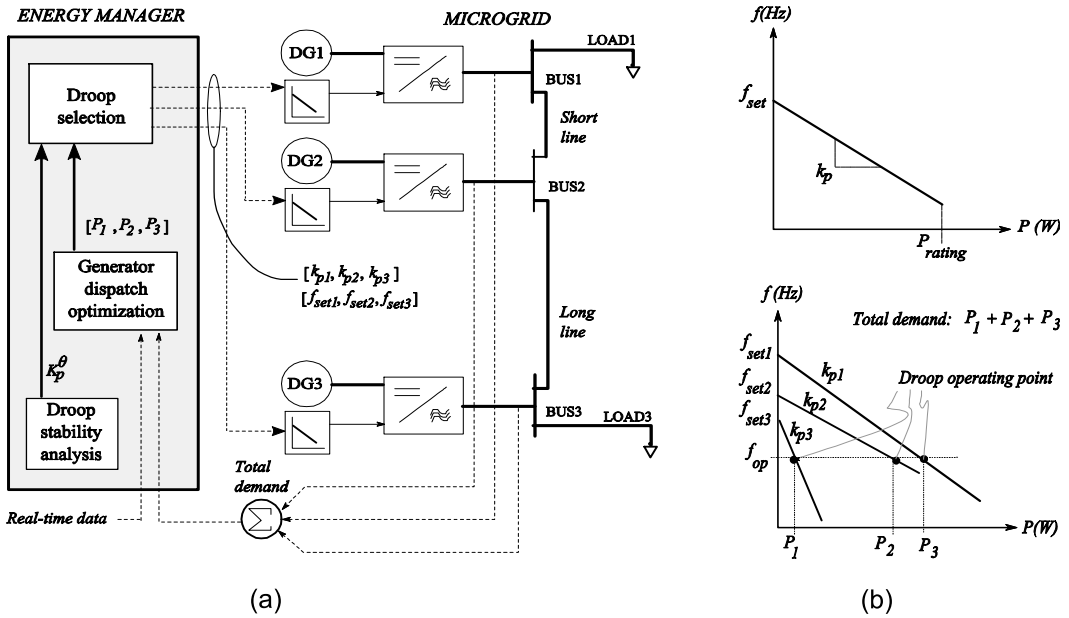

Fig. 1. Microgrid: (a) architecture and (b) frequency control

two sets of droops: real power vs. voltage frequency and reactive power vs. voltage magnitude. The real power droop, of particular interest here, is characterised by a frequency set point f_{set} and a droop gain k_p (Fig. 1). The generator rating P_{rating} limits the extent to which the droop is applicable.

When connected in parallel, generators share real power demand according to their combined droops. This determines the system operating frequency f_{op} (Fig. 1 (b)). To implement a particular droop operating point - with a certain power sharing at a chosen frequency - an EMS, in real time, can therefore adjust the generator droop settings relative to each other.

The microgrid studied in this paper is a three-phase balanced system with all generators and loads being balanced three-phase entities. Although out scope of this paper, it is worth mentioning that in a practical scenario a microgrid might include single-phase generators and loads resulting in unbalanced network conditions. The droop-based power controllers of the three-phase inverters, studied in this paper, use low-pass filters to eliminate the double frequency components (and harmonic components) in the measured power that result from these unbalanced conditions. This means the three-phase DG inverters are controlled to share only the fundamental-frequency balanced portion of the loads. Further research is needed to model and study unbalanced system conditions and to determine a suitable sharing/dispatch strategy where unbalance is significant.

III. EMS Design

Three functions form the proposed EMS, which is implemented on a PC: droop stability analysis, droop selection, and generator dispatch optimization (Fig. 1 (a)). The control loop, which consists of the two latter on-line functions, optimizes the generator power sharing approximately every 15 seconds by communicating new droop settings, based on demand read back from the inverter outputs. Droop stability analysis is carried out off-line.

A. Droop stability analysis

The droop stability analysis uses a small-signal state space model of the prototype microgrid. Such a model has been presented in full in [4], where analysis has shown that the dominant low-frequency eigenvalues are influenced primarily by the elements of the real power controller, and in particular by the frequency-droop gains k_p (Hz/W). These affect both system stability and transient performance. While a thorough analysis of droop gains in terms of transients would also be useful, the work presented here focuses on the relationship between droop gains and stability margins.

Fig. 2 illustrates the motion towards the imaginary axis of the two dominant eigenvalue pairs as k_p is increased, for a case when all inverters employ the same droop settings. f_{set} is also adjusted alongside k_p, to keep the droop operating point fixed; the EMS would similarly adjust both parameters, to achieve desired generator power outputs and operating frequency. Fig. 2 shows that a high droop gain makes the microgrid less stable, with instability occurring at k_p^{max}. For $k_p < k_p^{max}$ each droop gain can be annotated as k_p^{θ}, with a corresponding stability margin of angle θ. This angle is also shown in Fig. 2, and decreases as k_p increases. Based on this, an EMS could limit k_p to some k_p^{θ} to achieve a desired level of damping.

However, the eigenvalues in Fig. 2 are specific to a particular microgrid operating point, due to the small-signal analysis. k_p^{θ} and k_p^{max} change in real-time with the power flow. Rather than the EMS constantly recalculating these values, a more practical approach is to identify qualitatively the situations that limit k_p^{max} the most. This information can be used to construct a limit case, with a set of k_p^{θ} and k_p^{max} defined with capital letters as K_p^{θ} and K_p^{max}. For a particular K_p^{θ}, any operating condition within the extent of the limit case would then be assumed to exhibit at least the corresponding stability margin θ. The stability analysis can therefore be carried out off-line.

1) Limit case analysis : For the limit case analysis, two methods are used. Firstly, it is observed that the microgrid is less damped when all inverters have the same k_p, than if one or more inverters have

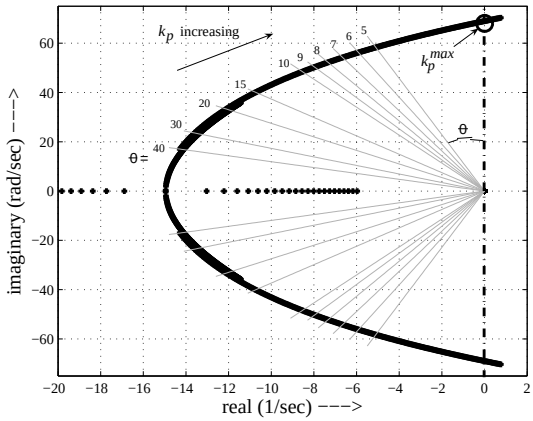

Fig. 2. Path of dominant eigenvalues as k_p increases, and corresponding stability margin θ (degrees)

droop gains below this value [13]. This can be confirmed from Fig. 3, which depicts the trace of two dominant eigenvalue pairs (marked as λ_{1-2} and λ_{1-3}). It can be seen that each unit has a different stable range for their droop gain. In this particular case, the droop gain of the second unit, k_p^2, has the lowest stable range. Equal droop gains are therefore used to compare the effect of different parameter values and operating conditions on k_p^{max}.

The choice of limit case, described here, is based on prior system knowledge. If the system is very large then choosing a limit case can be difficult. Having said that, it is a general practice to analyse a given system based on the prior knowledge and some engineering sense. Also, in general a microgrid is a small section of a big network with a limited number of possible configurations and network conditions and hence choosing a limit case shouldn't be too difficult.

Secondly, the change in k_p^{max} that results from such variations is studied with respect to a reference case (Fig. 4). In the reference case, the demand is at 50% of installed capacity, evenly divided between BUS1 and BUS3, and shared equally among the inverters at an operating frequency of 50 Hz.

From this reference baseline, it can be observed that k_p^{max} is lower for certain operating conditions (lower operating frequency, higher demand, and a larger proportion of the load on BUS3 (the end of the long line)). Higher value of line resistance also reduces k_p^{max}. Generator load sharing has a less straightforward effect. Results show that k_p^{max} is lower when DG1 supplies a large proportion of the demand, for inverter output powers down to 0.5 kW. The largest variation of k_p^{max} with respect to the reference case (approximately 8%) arises from the variation of line inductance but this is a relatively small

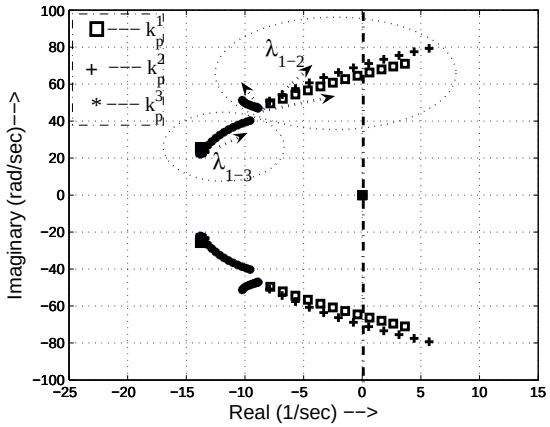

Fig. 3. Trace of dominant modes (λ_{1-2} and λ_{1-3}) as a function of individual droop gain of each inverter (arrow indicates the direction of increasing k_p)

variation and supports the approach of using a single K_p^θ and K_p^{max} in the EMS. It should be noted that the base case is a planning choice and this can vary from system to system. If we chose another base case the values in Fig.4 would change but modeling of the microgrid suggests that the basic behaviours would be the same.

Based on Fig. 4, the limit case considered here is: DG1 generates at full capacity (10 kW) while DG2 and DG3 generate near zero capacity (0.5 kW), at a low operating frequency (49.5 Hz), and with all load placed at BUS3. Fig. 5 shows how K_p^θ varies with stability margin θ for this situation. Droop gain versus stability margin is also shown for the reference case, and when the limit case has been extended to include worst-case variation in impedance values (assumed to be resistances +10$\%$ and inductances -5$\%$). These plots diverge more at low stability margins; the biggest difference in droop gain occurs at $\theta = 0$ degrees. At this point, the effect of impedance variations with respect to the limit case can be expressed as $\Delta K_p^{imp} \approx -2.7 \times 10^{-6}$ (Hz/W). This factor can be used to account for such effects in the stability analysis.

2) Experimental validation of limit case analysis: The laboratory microgrid was operated according to the limit case, in order to compare its stability performance with that of the small-signal model. Dominant eigenvalues were approximated from load step changes, by visually identifying the oscillation frequency and exponential decay of the inverter power output. At $k_p = 2.51 \times 10^{-5}$ (Hz/W), the shape of this response (shown in Fig. 6 as a relative change from an initial value) has a frequency of 7.7 Hz and a decay constant of 1.75, giving an eigenvalue with a stability margin of $\theta \approx 2$ degrees. Additional

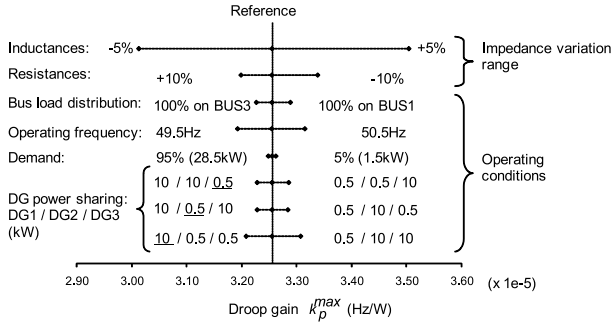

Fig. 4. Comparison of the variation in k_p^{max} with changes in impedances and operating conditions

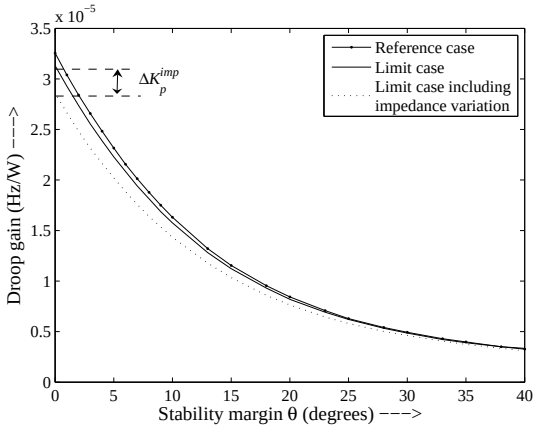

Fig. 5. Droop gain of reference case (k_p^θ) and limit case (K_p^θ) versus stability margin θ, based on small-signal analysis. $\Delta K_p^{imp} \approx -2.7 \times 10^{-6}$ (Hz/W).

droop gains yield eigenvalues that correspond to the stability margins θ in Fig 7. Although slightly less damped, the experimental setup agrees well with the model limit case. When shifted down, the simulated curve is a visual fit of the experimental data in the shown region of stability margins. The shift is $\Delta K_p^{exp} \approx -2.3 \times 10^{-6}$ (Hz/W).

To further test the validity of the limit case, the microgrid was again run according to limit case settings, except the operating frequency f_{op}: this was varied from above, to just below, 49.5 Hz. $k_p = 2.6 \times 10^{-5}$ (Hz/W) was chosen to place the limit case operation, occurring at 49.5 Hz, on the edge of instability. When adjusted by ΔK_p^{imp} and ΔK_p^{exp}, Fig. 7 shows that this droop gain corresponds to $K_p^\theta = 3.1 \times 10^{-5} \approx K_p^{max}$. As a lower f_{op} reduces k_p^{max} (Fig 4), the analysis suggests that the microgrid is likely to become unstable for f_{op} below 49.5 Hz. Fig 8 confirms this: the inverter power outputs become increasingly oscillatory until one inverter finally cuts out.

These results suggest that it is possible to ensure a stability margin of $> \theta$ degrees in the laboratory

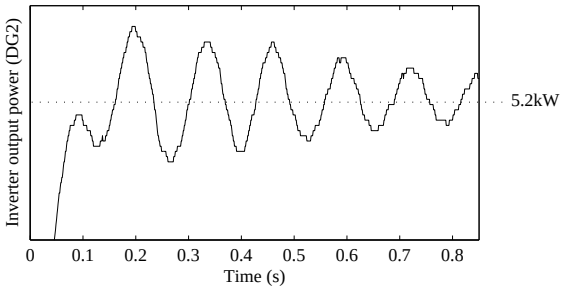

Fig. 6. Step response shape for $k_p = 2.51 \times 10^{-5}$ (Hz/W). The dominant eigenvalue gives a stability margin $\theta \approx 2$ degrees

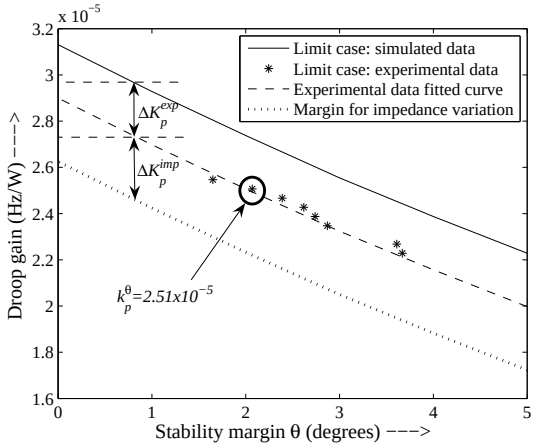

Fig. 7. Droop gain versus stability margin θ at limit case operation, for experimental (k_p^θ) and simulated small-signal analysis (K_p^θ) data. $\Delta K_p^{exp} \approx -2.3 \times 10^{-6}$

microgrid by applying the corresponding ΔK_p^θ from the model limit case, adjusted by ΔK_p^{exp} and ΔK_p^{imp} to account for the small modeling inaccuracies and impedance variations. Some limitations should be noted, however. Firstly, while ΔK_p^{imp} compensates for impedance variations in the choice of K_p^θ, the value obtained for ΔK_p^{exp} is also subject to such inaccuracies as well as to errors in the approximation of eigenvalues from step responses. Such errors are difficult to eliminate completely, and are often dealt with in the field by selecting a slightly larger stability margin than calculated theoretically.

Secondly, the value used for ΔK_p^{exp} is based on a narrow range of small stability margins. Since Fig. 5 shows that different operating cases diverge more in this range, however, it is reasonable to assume that the difference between the model and the experimental microgrid diminishes at larger stability margins.

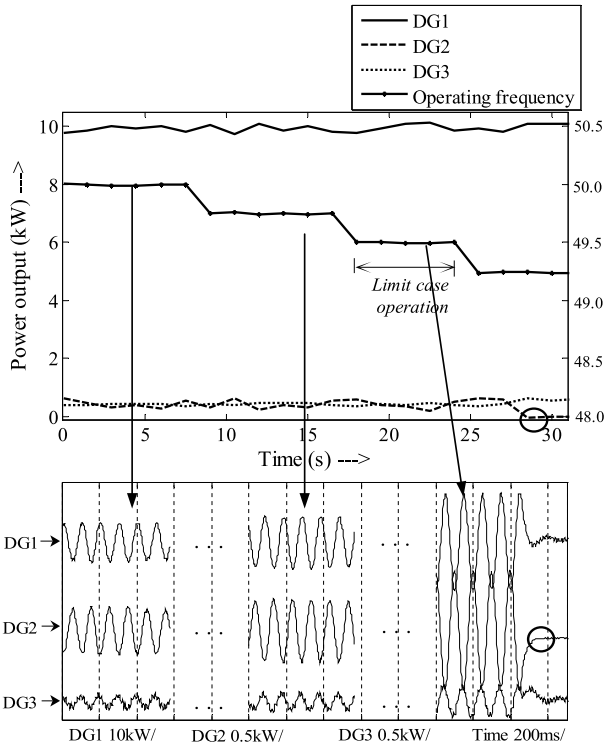

Fig. 8. Measured inverter power outputs as operating frequency is moved beyond the limit case for $k_p = 2.6 \times 10^{-5}$ (Hz/W)

Finally, the above stability analysis is specific to the chosen limit case and therefore does not consider, for example, operating frequencies below 49.5 Hz. However, the method proposed in this paper can easily be extended to incorporate additional operating conditions and factors, including non-linear loads, off-line generators, generator dynamics, or different network topologies that may arise due to line outages.

B. Inverter Droop Selection

A desired droop operating point - with a particular generator power sharing (P1, P2, P3) and system frequency f_{op} - can be achieved with a range of combinations of droop characteristics (Fig. 1 (b)). These options differ with regard to system performance. While high gains k_p reduce the stability margin (Fig. 2), low gains increase the response time, which results in poor transient behaviour in terms of higher energy storage requirements to deal with increased transient energy exchange. The settings also determine how the droop operating point moves in response to external influences such as load changes. For instance, high gains can force a significant step in operating frequency in response to a load change. Similarly, droop gains may prompt a generator that operates near maximum or zero dispatch to exceed its rating or absorb power, which requires appropriate control or protection measures. Consequently, the choice of

droops is a trade-off between stability margin, dynamic performance, and shifts in the droop operating point.

One straightforward method to select droops is to set identical gains k_p in all generators, based on this trade-off. Generator power sharing then becomes decoupled, determined only by the frequency set points f_{set}. For a chosen k_p, f_{set} is calculated for each generator as in equation (1) based on a suitable operating frequency f_{op} and the optimal generator output P_i requested by the dispatch optimization. This method is employed in the EMS proposed here. However, equal k_p force generators to share equal in any change in load power until the EMS's next re-dispatch action. This is not necessarily desirable. Alternative approaches can be envisaged where non-identical droop gains are used to restrict changes in power output of particular generators or tailor the system performance in other ways.

$$f_{set} = f_{op} + k_p \ . \ P_i \tag{1}$$

Reactive power droop gain is selected as a compromise between two contradicting requirements; a high droop gain for better transient response where as low droop gain for better voltage regulation. Also, due to high R/X ratio of low voltage cables active and reactive power control is not completely decoupled and a precise reactive power sharing can not be achieved [13],[14],[15]. Some solutions were already reported to over come this problem, such as the one presented in [16]. Sometimes a large variation to voltage magnitude (and hence large value for reactive power droop gain) can also give a better reactive power sharing. However, since the microgrid system stability is less affected by reactive power droop gain compared to real power droop gain (as explained in ref. [4] and [13]), and the focus of the paper is on economic dispatch of real power in a stable manner, the reactive power droop gains are kept constant throughout this work

C. EMS - Generator dispatch optimization

A generator dispatch optimization is included in the EMS to demonstrate the implementation of several power sharing scenarios. For this purpose the fuel minimization problem formulation in equation (2) is sufficient, although more extensive problem formulations or other methods may be appropriate, including issues such as generator dynamics or using real-time data such as fuel or energy pricing. The algorithm finds the optimal dispatch factor x_i for each generator *i*, which is a fraction between 0 and 1 of the

generator capacity P_{rating_i}. Constraints ensure that power (P^e_{demand}) and heat demands (P^h_{demand}) are met, where the heat generated depends on the Power-to-Heat Ratios (PHR) of available CHP generators. They also include restrictions on the generator dispatch factors: an upper bound (UB) to maintain a fast reserve, as is common in traditional power systems, and a lower bound (LB), because a switched off generator has not been covered by the stability analysis and may jeopardize the stability of the system.

$$\begin{aligned} & \min_{x_i} \ \{\sum_{i=1}^{3} = F_{rate_i}(x_i)\} \\ subject\ to \quad & \sum_{i=1}^{3} P_{rating_i} \ . \ x_i = P^e_{demand} \\ & \sum_{i=1}^{3} P_{rating_i} \ . \ (1/PHR_i) \ . \ x_i \ \geq \ P^h_{demand} \end{aligned} \tag{2}$$

The fuel consumption rates F_{rate} for the optimization algorithm (Fig. 9) have been taken from the technical datasheets of a 100kW microturbine (MTU) [17] and two 300 kW gas engines [18]. The 100 kW microturbine data has been fitted as a 4th order polynomial and scaled linearly with output power to represent a 200 kW unit. Similarly, the 300 kW gas engine data has been approximated by linear functions and then scaled to a 400 kW lean-burn and a 200 kW rich-burn engine. Dispatch factors for these hypothetical units are applied to the 10 kW inverters, to implement the power sharing on the microgrid. DG1 and DG2 represent the 400kW and 200 kW gas generators, while DG3 represents the 200 kW MTU.

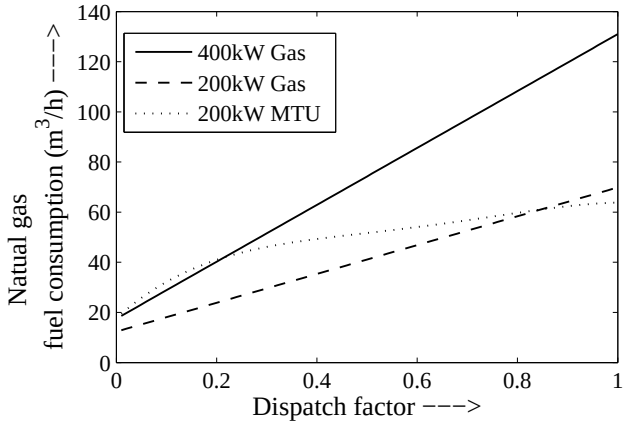

Fig. 9. Generator fuel consumption rates

IV. EMS EXPERIMENTAL VERIFICATION

Stable microgrid operation and the function of the complete EMS have been verified, for optimal dispatch of the units described in the preceding section. Dispatch factors (constrained by lower and upper bounds of 0.1 and 0.9 respectively) and output powers are shown in Fig. 10, for loads of 20-85$\%$ of installed capacity. The microturbine is assumed to have a Power-to-Heat Ratio of 0.6. Heat demand is set to 50$\%$ of its thermal capacity; it is consequently required to operate at a dispatch factor $\geq$ 0.5. As expected, the 400 kW lean-burn gas engine is preferred over the less efficient 200 kW unit.

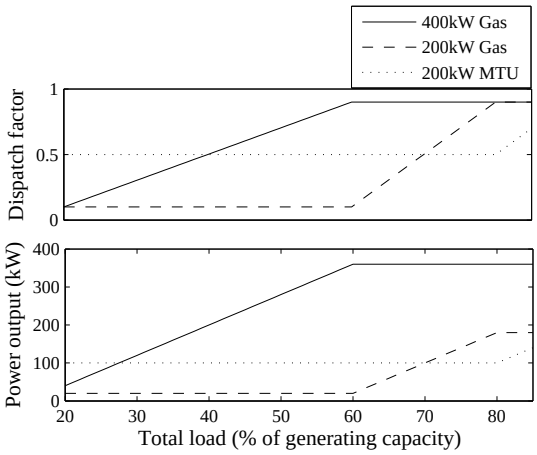

Fig. 10. Optimal dispatch factors and power outputs at 50$\%$ heat demand

In the droop selection, equal droop gains were used in all inverters ($k_p = 2.39 \times 10^{-5}$ (Hz/W)). Adjusting for ΔK_p^{imp} and ΔK_p^{exp}, this value corresponds to $K_p^{\theta} = 2.89 \times 10^{-5}$ (Hz/W) with a stability margin of $\theta \approx$ 1.25 degrees (Fig. 7). A larger margin would normally be selected, to avoid events such as tripping of generators due to a transient over shoot, but a low margin was chosen here to show that the microgrid's stability is maintained even in the worst case scenario. Frequency set points f_{set} were selected to give an operating frequency $f_{op} \approx$ 49.5 Hz at the optimal generator power outputs, from equation (1). As in the limit case in the stability analysis, the full load was applied on BUS3 and DG1 (the 400 kW gas engine) supplied most of the load at high demands.

Fig. 11 shows the stable outputs of the microgrid inverters as the load is increased progressively from 20$\%$ to 80$\%$ of the (scaled) generating capacity. The output profiles reflect the fact that inverters initially react to a load change based on their existing droops (point B). Within one EMS communication cycle, these droops - and hence power outputs - are adjusted to reflect updated optimal dispatch levels (point

C). The profile shapes can be compared to the optimal power levels in Fig. 10.

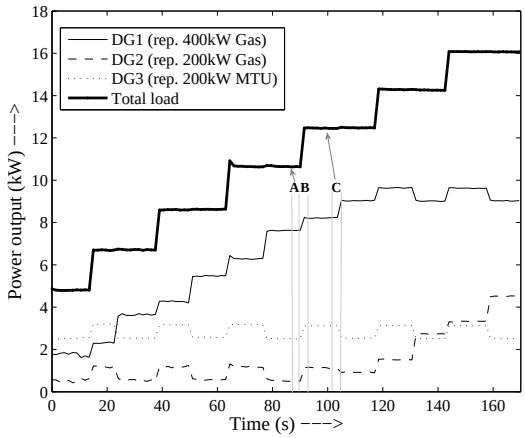

Fig. 11. Measured inverter power outputs during EMS optimal dispatch. (A) droop update : no change, (B) load change: new non-optimal outputs, (C) droop update : new optimal outputs

V. Conclusions

This paper has described an Energy Management System (EMS) for a droop-controlled stand-alone microgrid, which successfully implements optimal generator dispatch levels by selecting droops from a region where the stable operation of the microgrid can be guaranteed. Three key elements make up the proposed EMS: droop stability analysis, droop selection, and generator dispatch optimization. The stability analysis stage illustrates an ‘off-line’ method of identifying the stability constraints imposed by droop characteristics, using a small-signal approach. Droop selection then identifies a specific set of droop characteristics from the stability-guaranteed region, in order to implement optimal power outputs. The required power outputs are provided by the optimal generator dispatch, which effectively is a fuel optimization algorithm aimed at reducing the operating costs of the microgrid.

Particular emphasis has been paid to the impact of droop gains on stability, because these parameters have been found to play a significant role in the microgrid’s dynamic performance. The proposed analysis is based on the use of a sufficiently accurate small-signal model and a limit case to establish a single stability constraint. Experimental data has been presented that supports the validity of these methods. Other operating conditions, such as off-line generators or different network topologies that may arise due to line outages, can be incorporated in the analysis to extend its use. Finally, by providing a deeper understanding

of microgrid stability, the proposed analysis may make it feasible to implement more sophisticated DG droop settings in stand-alone microgrids, to further improve their performance.

REFERENCES

[1] C. Marnay, A. S. Siddiqui, and F. J. Rubio, "Shape of the microgrid," *Proc. IEEE Power Engineering Society Winter Meeting, Columbus*, pp. 150–153, Jan/Feb 2001.

[2] S. Abu-Sharkh, "Can microgrids make a major contribution to the uk energy supply," *Renewable and Sustainable Energy Reviews*, vol. 10, no. 2, pp. 78–127, April 2006.

[3] R. H. Lasseter, "Microgrids," *Proceedings of the IEEE Power Engineering Society Winter Meeting*, vol. 1, pp. 305–308, Jan. 2002.

[4] N. Pogaku, M. Prodanovic, and T. C. Green, "Modeling, analysis and testing of autonomous operation of an inverter-based microgrid," *IEEE Transactions on Power Electronics*, vol. 22, no. 2, pp. 613–625, March 2007.

[5] F. Katiraei and M. R. Iravani, "Power management strategies for microgrid with multiple distributed generation units," *IEEE Transactions on Power Systems*, vol. 21, no. 4, pp. 1821–1831, Nov 2006.

[6] C. A. Hernandez-Aramburo, T. C. Green, and N. Mugniot, "Fuel consumption minimization of a microgrid," *IEEE Transactions on Industry Applications*, vol. 41, no. 3, pp. 673–681, May/June 2005.

[7] R. H. Lasseter, "Integration of distributed energy resources: The certs microgrid concept," *Lawrence Berkeley National Lab., CA, Report No. LBNL-50829*, April 2002.

[8] R. Firestone and C. Marnay, "Energy manager design for microgrids," *Lawrence Berkeley National CA., USA, Report No. LBNL-54447*, Jan 2005.

[9] A. L. Dimeas and N. D. Hatziargyriou, "Operation of a multiagent system for microgrid control," *IEEE Transactions on Power Systems*, vol. 20, no. 3, pp. 1447–1455, Aug 2005.

[10] J. Oyarzabal, J. Jimeno, J. Ruela, A. Engler, and C. Hardt, "Agent based microgrid management system," *Proc. International Conference on Future Power Systems*, pp. 1–6, Nov 2005.

[11] D. Pudjianto, G. Strbac, F. van Overbeeke, A. I. Androutsos, Z. Larrabe, and J. T. Saraiva, "Investigation of regulatory, commercial, economic and environmental issues in microgrids," *Proc. International Conference on Future Power Systems*, Nov 2005.

[12] E. Handschin, F. Neise, H. Neumann, and R. Schultz, "Optimal operation of dispersed generation under uncertainty using mathematical programming," *International Journal of Electrical Power and Energy Systems*, vol. 28, no. 9, pp. 618–626, Nov 2006.

[13] N. Pogaku, "Analysis, control and testing of inverter-based distributed generation in standalone and grid-connected applications," Ph.D. dissertation, Imperial College London, University of London, 2006.

[14] J. A. P. Lopes, C. L. Moreira, and A. G. Madureiara, "Defining control strategies for microgrids islanded operation," *IEEE Transactions on Power Systems*, vol. 21, no. 2, pp. 916–924, May 2006.

[15] C. L. Moreira, F. O. Resende, and J. A. P. Lopes, "Using low voltage microgrids for service restoration," *IEEE Transactions on Power Systems*, vol. 22, no. 1, pp. 395–403, Feb 2007.

[16] K. D. Brabandere, B. Bolsens, J. V. den Keybus, A. Woyte, J. Driesen, and R. Belmans, "A voltage and frequency droop control method for parallel inverters," *IEEE Transactions on Power Electronics*, vol. 22, no. 4, pp. 1107–1115, July 2007.

[17] EEA, "Technical datasheets for TA100 microturbine," Elliott Energy Systems, Tech. Rep.

[18] ——, "Technical datasheets for 400GSW gas based generators detroit diesel," Elliott Energy Systems, Tech. Rep., Dec 2006.